Using the 3D Vector Antenna as the Short-Range Direction-Finding Sensor: Primary Theory and Experimental Proof

Hadeel Obaid[1*], Christophe Morlaas[2*], Bo Sun[1], Matias Turunen[1], Simona Lohan[1**], Bo Tan[1*]

[1] *Faculty of Information Technology and Communications Sciences, Tampere University, Finland*
[2] *ENAC, Université de Toulouse, France.* [*] *Member, IEEE,* [**] *Senior Member, IEEE*

Abstract—This work showcases the design, implementation, and verification of a vector antenna (VA) capable of direction finding. By adopting the tapered slot (also known as Vivaldi) element as the constitutive VA element and a four-season layout, the VA in this work can identify the radio source in a wide spectrum range in the three-dimensional space. Practical issues, such as steering vector calibration, exploitation of polarization, and angle estimation with partial electromagnetic measurements, are addressed to ensure the functionality of the proposed VA in practice. A four-channel phase-locked software-defined radio platform and quasi-real-time angle estimation algorithms are designed and implemented to verify the direction-finding (DF) capability of the VA for directly propagated, reflected, and diffracted radio signals, respectively. The results of the experiment prove the effectiveness of the theory and our practical VA measures for 3D direction finding under various conditions and potentially inspire localization, mapping, and navigation in short-range scenarios.

Index Terms—Direction finding, Vector Antenna, Polarization, Angle of Arrival, Line-of-Sight, Non-Line-of-Sight, Obstacled-Line-of-Sight.

I. INTRODUCTION

Radio Direction Finding (RDF) has a long history of navigation. The RDF solutions, such as Automatic Direction Finders (ADF), Nondirectional Beacons (NDB), and Long-Range Navigation (LORAN), played vital roles in maritime and aviation craft navigation. With GNSS taking over conventional RDF systems, modern RDF applications now shift from navigating long-distance boats and planes to handling short-range cases, for example, localizing and tracking users or interference sources in the mobile system [1], angle-based indoor location estimation based on Bluetooth signal [2]. The modern RDF system often uses phased array antennas, which operate at the higher carrier frequency and allow beamforming for more accurate and faster direction estimation.

The phased array receiver can identify the direction of arrival (DoA) of the wavefront by exploiting the relation between the phase rotating pattern and wavefront striking angle. There have been various well-proven methods for DoA estimation, including Multiple Signal Classification (MUSIC) and its variants such as root-MUSIC, Estimation of Signal Parameters via Rotational Invariant Techniques (ESPRIT), etc. Most covariance-matrix-based and subspace-based RDF methods can achieve direction estimations in multiple dimensions (azimuth, elevation) and high angular resolution by extending the array layout dimensionality and physical array aperture. However, acquiring the above-mentioned benefits causes extra costs due to increased design and implementation complexity. In addition, subspace techniques suffer performance degradation caused by other inherent imperfections, such as mutual coupling between the array elements [3] or the randomness of the element failure [4]. To rule out the limitations of the phased-array-based solution in RDF, we explore the potential of a three-dimensional vector antenna (VA) for the DF problem. A VA consists of two orthogonal triads of scalar elements that measure the electric and magnetic field component [5]. The DoA of an incoming electromagnetic (EM) wave can be derived from the measurement of electric components (e_z, e_x, e_y) and magnetic components (h_z, h_x, h_y) that can be measured directly from the VA radiating elements [6], or indirectly calculated from the weighted signals received by the relevant constitutive radiating elements [7]. VA gains potential ascendancy by exploiting all available electromagnetic information with a smaller aperture in 3D and maintaining functionality with element failure.

The research effort in investigating the DF capability of VA is notably limited. Researchers in [8] present a novel closed-form ESPRIT-based algorithm that leverages the VA for DF and polarization estimation and verifies the results using simulation. Then in [9], a prototype for designing a vector sensor with fewer antenna elements is developed. In [10], a VA with fewer antenna elements is introduced by proposing a feeding network. Duplouy et al. use full-wave EM simulations for experimental validations to predict the direction-finding performances of the VA in [11]. Then they reported measurement results to experimentally validate the benefits of radiation diversity offered by the 2-season VA in DF performances in [7] and made modifications to the feeding circuit and incorporated a horizontal EM sensor of the 2-season VA to enhance the DF performance in [12]. In this study, we describe the design and experimental verification of a VA capable of direction-finding radio signals in a wide range spectrum. The highlights of this work can be expounded from the following aspects:

- Design and implementation of a novel compact size four-season wideband VA capable of simultaneous estimating azimuth and elevation angles of the direct or indirect propagated radio signals;
- The identification and resolution of the practical problems involved in the aforementioned design, namely the steering vector calibration, the exploitation of the signal polarization, and the incomplete constitutive radiating measurements that impact the DF functionality and performance of a VA;
- A fully functional, four-channel, phase-locked software-defined radio (SDR) system is designed together with the quasi-real-time DF algorithm to verify the function of devised 3D VA;
- Three experiment/in-lab scenarios are proposed and implemented to verify the capability of the VA for 3D direction estimation and identify the directions of radio signals from various conditions, including direct, reflecting, and diffracting propagation. Our experimental results in the uncontrolled laboratory environment prove we can achieve the 3D RDF by only using partial-port outputs for vertical and horizontal polarization radio sources.

II. THEORY AND PRACTICALITY OF THE VA

A. Principle of VA Design and DF

Theoretically, a VA is a six-component point-like sensor consisting of three identical, orthogonally orientated electric dipoles (dipole triad)

This work was supported by EU/SESAR Joint Undertaking in project NewSense (893917). This work was also partly supported by the Academy of Finland ULTRA (328226) and Business Finland 5G-PSS (6868/31/2021).

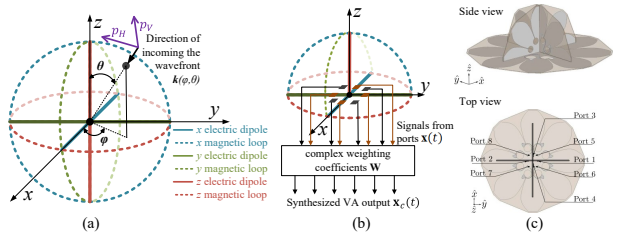

Fig. 1. 3D layout of the electric and magnetic elements of a 6-ports VA in original theory (a), the schematic of constitutive radiating elements based 8-ports VA (b) and an example of a wideband four-season 8-ports Vivaldi VA implementation (c) [12], with 33 cm diameter.

and three identical, orthogonally orientated magnetic loops (loop triad). The electric-dipoles triad and the magnetic-loop triad are used for measuring (e_z, e_x, e_y) and (h_z, h_x, h_y), respectively. The 3D layout of the six components is shown in Fig 1 (a).

Let $\mathbf{k}(\theta,\phi)$, $\mathbf{p}(\mathbf{p_V},\mathbf{p_H})$ be the wave direction vector and the polarization vector of the transverse incoming plane wave $s(t)$ (in the nonconductive homogeneous isotropic medium) at the VA, $\theta \le \pi/2$ and $\phi \in [0, 2\pi)$. $\mathbf{p_V}$ and $\mathbf{p_H}$ are orthogonal to each other, and both are orthogonal to the wave direction vector $\mathbf{k}(\theta,\phi)$ as shown in Fig. 1 (a). According to the VA signal model in [5], the waveform incident $\mathbf{x}(t) \in \mathbb{C}^6$ of the six-component VA consists of three electric fields and three magnetic field measurements in Cartesian coordination, which are jointly determined by wave direction and polarization status. Thus, the VA outputs $\mathbf{x}(t)$ can be expressed as: $\mathbf{x}(t) = \mathbf{d}(\phi,\theta,\gamma,\eta)\cdot s(t) + \mathbf{n}(t)$, where $\mathbf{n}(t) \in \mathbb{C}^6$ is the spatially invariant, zero-mean additive white noise at time t, $\mathbf{d}(\phi,\theta,\gamma,\eta) \in \mathbb{C}^6$ is the VA response associated with incoming wave direction vector $\mathbf{k}(\theta,\phi)$, which can be written as the vector form as (1):

$$\mathbf{d}(\phi,\theta,\gamma,\eta) = \begin{bmatrix} e_x \\ e_y \\ e_z \\ h_x \\ h_y \\ h_z \end{bmatrix} = \begin{bmatrix} \cos\phi\cos\theta & -\sin\phi \\ \sin\phi\cos\theta & \cos\phi \\ -\sin\theta & 0 \\ -\sin\phi & -\cos\phi\cos\theta \\ \cos\phi & -\sin\phi\cos\theta \\ 0 & \sin\theta \end{bmatrix} \begin{bmatrix} \sin\gamma e^{i\eta} \\ \cos\gamma \end{bmatrix}, \quad (1)$$

where $\gamma \in [0, \pi/2]$ and $\eta \in [-\pi/2, \pi/2]$ refer to the auxiliary polarization angle and the polarization phase difference, respectively. In the original VA design, the measured signal $\mathbf{x}(t)$ from the six ports directly reflects the intensity of electric fields and three magnetic fields caused by the incoming radio wave. This fact is different from the indirect VA design in Section II B. Analogously to the steering vector of the scalar sensor array, the VA response $\mathbf{d}$ can also be applied in the subspace-based method to find the direction of radio sources, typically MUSIC. MUSIC-based DF can be briefly implemented by following the processing from (2) to (3). With the VA output $\mathbf{x}(t)$, the covariance matrix is:

$$R_{\mathbf{xx}} = \mathbb{E}[\mathbf{x}(t)\mathbf{x}^*(t)], \quad (2)$$

where $\mathbb{E}[\cdot]$ denotes expectation, $(\cdot)^*$ indicates the conjugate transpose. Then, eigenvalue decomposition is applied on $R_{\mathbf{xx}}$; $\lambda = [\lambda_1, \lambda_2, ..., \lambda_6]$ is the eigen-value vector in ascending order and $E = [\mathbf{e}_1, \mathbf{e}_2, ..., \mathbf{e}_6]$ is the eigenvector matrix, formed by the eigenvectors $\mathbf{e}_i$ associated with the eigenvalues λ_i. We assume there are N ($N \le 5$) significant eigenvalue values; N indicates the number of radio sources. Then, the noise subspace can be constructed by $E_n = [\mathbf{e}_1, \mathbf{e}_2, ..., \mathbf{e}_M]$, where $M = 6 - N$. Estimating the direction of the incoming wave direction $\mathbf{k}(\theta,\phi)$ can be converted into exhaustive searching of spaces orthogonal to the noise subspace. The process is equivalent to searching peaks on the MUSIC pseudo-spectrum over elevation and azimuth dimensions:

$$P(\theta,\phi) = \frac{1}{\mathbf{d}^*(\theta,\phi,\gamma,\eta)E_n E_n^* \mathbf{d}(\theta,\phi,\gamma,\eta)}. \quad (3)$$

In the cases where the polarization status is known, the VA response vector $\mathbf{d}(\theta,\phi,\gamma,\eta)$ in (3) can be simplified to $\mathbf{d}(\theta,\phi)$.

B. Radiating Elements Based VA Design

Besides the direct measuring from the dipole and loop triads, the electric and magnetic components can also be derived from other types of constitutive radiating elements indirectly, e.g., opposing-load loop (OLL) [13] or Vivaldi antenna setting [7]. The approach is effective if the weighting coefficients can be found and associated with signals measured from the radiating elements for synthesizing the radiation pattern (RP) of the dipole and loop triads. Fig 1 (b) and (c) show the schematic design and implementation of an 8-port VA based on Vivaldi antennas, which are the same as [12]. If we still use the symbol $\mathbf{x}_c(t) \in \mathbb{C}^P$ to denote the port output, where P is the number of ports ($P = 8$ in Vivaldi VA shown in the Fig. 1 (c)). The synthesized response can be denoted as: $\mathbf{x}(t) = \mathbf{W}\mathbf{x}_c(t)$, where $\mathbf{W} = [\mathbf{w}_1, \mathbf{w}_2, ..., \mathbf{w}_6] \in \mathbb{C}^{6,P}$ denotes the complex weighting coefficients[1] applied at the P ports of the VA. The process of equation (II-B) is to retrieve the original six electric and magnetic elements from the received signals of eight ports. Table 1 shows the required coefficients that synthesize RPs of dipole triads. Vivaldi antennas have been chosen because their radiating characteristics respect geometrical and electrical symmetry allowing to synthesize of the RPs of dipole triads for specific geometrical and feeding settings. Other radiating elements can also be used with proper arrangement and excitation. The advantage of Vivaldi antennas comes from wideband operation capabilities. The benefit of the indirect implementation of the VA is its two-fold flexibility: *i).* the RPs diversity brings the hardware simplicity. It allows an enhanced performance using advanced signal processing and, *ii).* the additional RPs potentially improve the DF accuracy for broadband operations. In Section III, we only take signals from 4 ports for RDF function verification.

TABLE 1. Set of weighting coefficients $\mathbf{W}$ for the 8-ports VA.

	E/H Component	Port 1	Port 2	Port 3	Port 4	Port 5	Port 6	Port 7	Port 8	
$\mathbf{W}$	$\mathbf{E}_x$	0	0	0	0	1	-1	-1	1	$\}$ 6
	$\mathbf{E}_y$	0	0	0	0	-1	-1	1	1	
	$\mathbf{E}_z$	1	1	1	1	0	0	0	0	
	$\mathbf{H}_x$	1	-1	0	0	0	0	0	0	
	$\mathbf{H}_y$	0	0	1	-1	0	0	0	0	
	$\mathbf{H}_z$	0	0	0	0	1	-1	1	-1	

C. Practicality of Vivaldi-Elements-Based VA

Contrary to most multiple-element EM sensor arrays for which the mutual coupling between the closely placed elements often causes performance deterioration [14], the VA exhibits few mutual coupling thanks to the EM orthogonality properties due to the point-like (i.e. collocated) nature of the radiating elements. However, some amplitude and phase distortions due to the feeding-network coupling and manufacturing tolerances persist and must be calibrated. To mitigate the impact of amplitude and phase distortions at the VA outputs, various calibration solutions are proposed in practice [15]. Furthermore, a steering matrix is needed for each θ, ϕ set covering a hemispheric field of view when using the MUSIC algorithm for AOA retrieval. This calibration matrix is based on the computation of the combined steering vectors $\mathbf{d}$ from the RPs of each VA radiating element. Then, the steering matrix is computed from these electric fields with $\mathbf{d}_k(\phi,\theta) = E_k(\phi,\theta)$, where $E_k(\phi,\theta)$ denotes the electric field radiated by the k_{th} antenna. Thus, the steering vector used in experimental verification (Section III) is calibrated based on full wave simulation as reported in [16].

[1] $\mathbf{W}$ is not a unique solution. The optimal $\mathbf{W}$ are difficult to find in a vast space.

III. EXPERIMENTAL VERIFICATION

A. Verification System and Environment

A four-channel phased-locked reconfigurable receiver is designed and implemented to verify the DF capability of the four-season Vivaldi VA. The verification system adopts two NI® USRP RIOs (2954) to downconvert and digitize constitutive radiating measurements from the four VA ports. Each USRP module contains two receiving channels. The OctoClock CDA-2990 is used to drive USRPs with a common 10MHz reference and pulse-per-second (PPS) trigger to ensure phase lock of multiple receiving channels during the experiment period. The raw-sample streams from the receiving channels are aggregated through the peripheral component interconnect express (PCIe) interfacing switch, CPS-8910, to a workstation (PC), where the LabVIEW® is installed for performing signal calibration and RDF. The DC offset, IQ imbalance, and random phase offset of multiple channel signals must be calibrated initially for angle estimation processing. The directional Yagi antenna (5 dBi gain, 45° beamwidth) is the signal source to reduce multipath impact. Based on the MUSIC algorithm, RDF performance is positively correlated with the number of snapshots used in (2) and is independent of the signal waveform. The experiment uses the 5G uplink Sounding Reference Signal which is the orthogonal frequency division multiplexing (OFDM) modulated Zadoff-Chu sequence. A 0dBm signal is transmitted on the 2.1 GHz carrier frequency with 15 kHz subcarrier spacing within a 10 MHz bandwidth. Both vertical and horizontal polarizations are included. 600 snapshots are used for performing the MUSIC algorithm. Fig 2 shows the verification system's key components and signal flow. The experiments occur in a

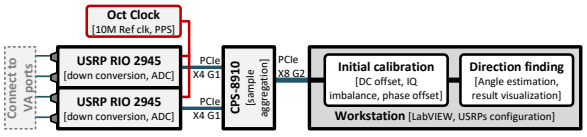

Fig. 2. The brief schematic of the verification system

normal uncontrolled laboratory environment without electromagnetic shielding. This indicates that there will be multipath scatterings from nearby objects (e.g., metal poles, walls, personnel, equipment chassis, and racks) beside the direct, reflected, or diffracted signals.

B. Experiment Scenarios

To verify the RDF capability under various conditions, in this work, three experimental scenarios are devised for distances ranging from 1 to 3.4 meters: *i*) RDF of line-of-sight (LoS) signal; *ii*) RDF of reflected signal; *iii*) RDF of obstructed line-of-sight (OLoS) signal (see Fig. 3). For the RDF of direct signal in Scenario (*i*), the joint azimuth and elevation angle estimation capability is verified, and the angle estimation accuracy is demonstrated against different propagation distances. For the RDF of the reflected and obstructed signals in Scenarios (*ii*)-(*iii*), we verify the azimuth angle discrimination capability of the reflected and diffracted signals with the fixed elevation angle. The reflector in Scenario (*ii*), also used as the obstacle in Scenario (*iii*), is a 0.1089 m^2 metal foil-covered styrofoam board.

C. Laboratory Measured Results

Due to the limited number of RF channels in the verification system, we can only use signals from 4 of the 8 VA ports. Benefiting from the reconfigurability of the radiating-element-based design, we are still able to verify the RDF capability with partial ports.

1) RDF of signal with horizontal or vertical polarization: To verify the RDF of the vertically polarized radio signal, the ports 1 ~ 4 of Vivaldi VA are configured to be active. Consequently, column 1 ~ 4 of the complex weighting coefficients matrix $\mathbf{W}$ is chosen to reconstruct the partial VA response (e_z, h_x, h_y). For the horizontally polarized radio

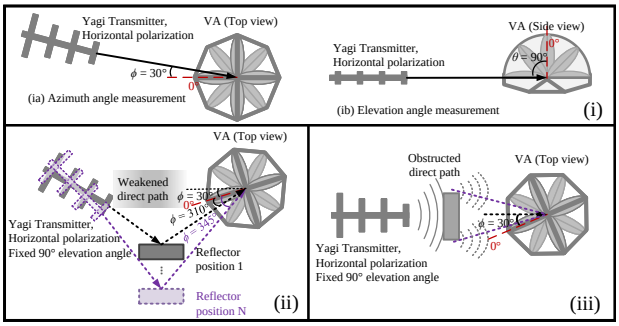

Fig. 3. Three experimental scenarios to verify the DF capability of the VA: i). RDF of direct transmission; ii). RDF of reflections; iii). RDF of the obstructed radio source.

signal, ports 5 ~ 8 are configured to be active. Column 5 ~ 8 of complex weighting coefficients matrix $\mathbf{W}$ are chosen to reconstruct the partial VA response (h_z, e_x, e_y). The results in Fig. 4 demonstrate that the Vivaldi VA can identify azimuth and elevation angles simultaneously. With the full configuration (using signals from 8 ports), the Vivaldi VA can be easily used for polarization-agnostic 3D RDF with better results due to a better description of the EM incoming field. We can see that

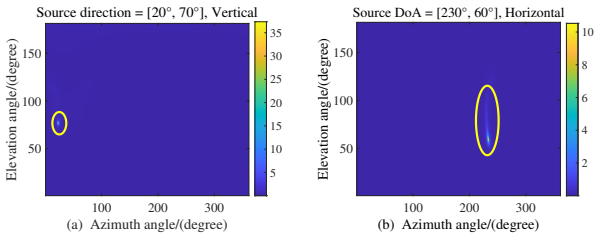

Fig. 4. Examples RDF: (a). a vertically polarized signal at $[\phi, \theta] = [20°, 70°]$; (b). a horizontally polarized signal at $[\phi, \theta] = [230°, 60°]$.

there is a "comet tail" in Fig.4 (b). The two potential reasons may cause the phenomenon: 1). Only the H_z field component can estimate the elevation angle. The radiation pattern presents a very low dynamic at the high elevation angle region; 2). It may also be because the ground multipath reflection has a stronger correlation with the direct signal in the horizontal polarization case.

2) RDF accuracy against varying distances: To ensure consistency, we use the same VA configuration (port 5 ~ 8) and radio source direction ($[\phi, \theta] = [30°, 90°]$) settings in the experiment Fig. 4 (b) which is also the same geometry layout as in Fig. 3 (i). We change the distance between the source and VA from 1 to 3.4 meters. The longer propagation distance will result in a larger angle estimation error in RDF because of the decreasing signal-to-noise ratio (SNR) caused by propagation attenuation. In Fig. 5 (a), we observe that the standard deviation for the estimation of the angle (STD) increases with the propagation distance, indicating a negative correlation between accuracy and distance. It is worth noticing that the far-field range of our experiment should be longer than 1.52 m according to the edge size of 33cm of the VA. The estimated direction at the 1 m transmission distance maintains good accuracy even in the near field. Constrained by the experiment venue, it is difficult to test the operation range limit of the designed Vivaldi-VA. Also, the actual operating range is determined by a series of factors, such as the accuracy requirement of services, transmitting power, and the propagation environment. Here, an indirect test is conducted. The main consequence of the extended range is the increasing variance in estimation caused by the decreased SNR. Thus, we use the lower transmitting power to mimic the longer range. The transmit power is further converted to the receiving SNR, $\Gamma = P_{tx} + l_0 - n_0(r_0)B$ by considering USRP hardware factors: the noise floor $n_0 = -145$ dBm/Hz at receiver reference level $r_0 = 0$ dBm over $B = 10$ MHz and the constant

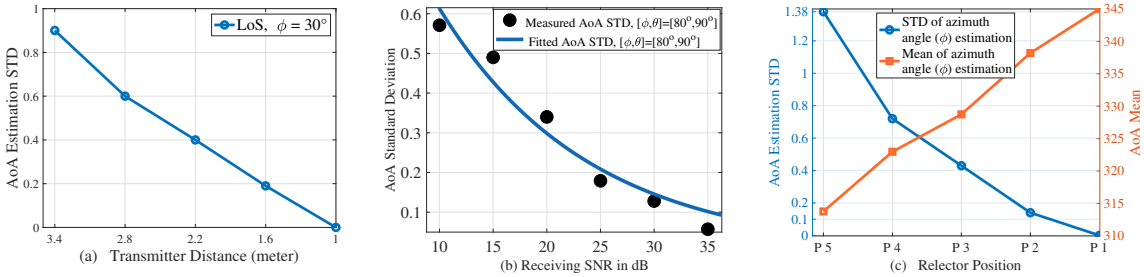

Fig. 5. The angle estimation performance of (a). LoS signal source in the different distances; (b). The measured and fitted AoA estimation STD against the receiving SNR; (c). reflector in different locations.

attenuation $l_0 = -55$ dB which is caused by hardware imperfection and propagation losses. l_0 value is measured based on our system and will change if the system configuration changes. In Fig. 5 (b), the STDs of measured AoA estimation at different SNR levels are shown together with the fitted exponential function $\sigma_{AoA}(\Gamma) = 1.26 \cdot e^{(-0.072 \cdot \Gamma)}$, where σ_{AoA} indicates the STD for the estimation of angle. The fitted function in Fig. 5 (b) provide information on AoA estimation that deteriorates with range extension (SNR decrease).

3) RDF of reflected radio signal: Besides verifying the RDF capability of the LoS signal source, we also verified the RDF of the reflected signal. As shown in Fig. 3 (ii), the main beam of the Yagi antenna is pointed in a direction away from the VA. A reflector is placed from position 1 (P_1) to position N (P_N) to redirect the main beam signal back to the VA. The arrival signal at VA is the summation of the reflected signal from the NLoS path, sidelobe leakage from the LoS path, and other multiple path signals. Due to the constraints of reflection area, signal coherence, and a limited degree of freedom (DoF) of the available signal space, it may be difficult to discriminate the direction of the reflected signal from the summation. We use the same VA configuration (port 5 ~ 8) in the experiment Fig. 4(b) for distinguishing the direction of the reflected signal. In Fig. 5(c), we observe that the VA can successfully identify the subtle changes of reflector direction with the presence of the coherent LoS leakage and other multiple signals by only using 4 port outputs (i.e. two electric and one magnetic component). The STD of the angle estimation increases from P_1 to P_N due to the increase in propagation distance, which is consistent with the observation in Fig. 4(a). The capability of estimating the reflector direction is a promising sign for mapping the indoor space.

4) RDF of obstructed radio signal: In the OLoS scenario shown in Fig. 3(iii), an obstacle is placed between the Yagi transmitter and the VA. As a result of diffracting propagation, partial signal energy may still arrive at the VA from the top or bottom edge of the obstacle. For an ideal direction finder, we should observe two arrival angles which are from the top and bottom edges to the VA center point, as the two purple lines are shown in Fig.3(iii)). However, our verification system only takes signals from four available ports, equivalent to three electromagnetic components. The maximum recognizable sources will be only two. The number of recognizable sources will be smaller due to the impact of coherence, multipath, antenna element coupling, and low power strength of the signal of interest. Therefore, we did not successfully identify the direction of the diffracted signal in the OLoS scenario with the experimental environment shown in Section III. B.

5) Comparison with the state-of-the-art: The remarkable aspect of this work is the verification of the VA-based RDF hypothesis through real-time DF experiments using a self-designed Vivaldi elements-based VA and MUSIC algorithm in an uncontrolled indoor environment. Most current studies are often conducted solely using simulations [8]–[11] or in controlled environments (e.g., anechoic chamber) [12]. It is difficult to identify the counterpart results, which are performed using the identical DF algorithm and VA configurations in similar environments for comparison. One future direction is to set up the referencing configuration and performance for VA-based RDF studies.

IV. CONCLUSION

We introduced the VA for the short distance and indoor RDF in 3D. Based on the premier 6-component vector sensor design, an 8-port four-season Vivaldi VA was designed and manufactured for RDF in the upper hemisphere. A 4-channel SDR-based system was designed and implemented for laboratory verification. Based on the measurements of three experimental scenarios, we proved that the VA is capable of *i).* the simultaneous estimation of the azimuth and elevation angle of the radio sources with vertical or horizontal polarization using only partial ports outputs and *ii).* identifying the direction of the reflected signal when coherent signals are present from other directions. The experimentally verified RDF function in different scenarios proves that VA is a promising option for multifarious applications such as indoor radio source localization and mapping.

REFERENCES

[1] R. L. Haupt, *Direction Finding*, pp. 301–323. John Wiley & Sons, Ltd, 2020.

[2] N. B. Suryavanshi and et al, "Direction finding capability in bluetooth 5.1 standard," in *Ubiquitous Communications and Network Computing*, pp. 53–65, Springer, 2019.

[3] B. Friedlander and A. Weiss, "Direction finding in the presence of mutual coupling," *IEEE Transactions on Antennas and Propagation*, vol. 39, pp. 273–284, 1991.

[4] H. Southall, J. Simmers, and T. O'Donnell, "Direction finding in phased arrays with a neural network beamformer," *IEEE Transactions on Antennas and Propagation*, vol. 43, no. 12, pp. 1369–1374, 1995.

[5] A. Nehorai and E. Paldi, "Vector-sensor array processing for electromagnetic source localization," *IEEE Transactions on Signal Processing*, vol. 42, pp. 376–398, 1994.

[6] K. Wong, "Direction finding/polarization estimation-dipole and/or loop triad(s)," *IEEE Transactions on Aerospace and Electronic Systems*, vol. 37, no. 2, 2001.

[7] J. Duplouy and et al., "Wideband and reconfigurable vector antenna using radiation pattern diversity for 3-d direction-of-arrival estimation," *IEEE Transactions on Antennas and Propagation*, vol. 67, no. 6, pp. 3586–3596, 2019.

[8] K. Wong and M. Zoltowski, "Closed-form direction finding and polarization estimation with arbitrarily spaced electromagnetic vector-sensors at unknown locations," *IEEE Transactions on Antennas and Propagation*, vol. 48, no. 5, pp. 671–681, 2000.

[9] J. Lominé, C. Morlaas, and H. Aubert, "Novel vector sensors design with three co-located or distributed elements for the 3d doa estimation," *Progress in Electromagnetics research B*, vol. 57, pp. 207–220, 2014.

[10] A. Chabory, C. Morlaas, R. Douvenot, and B. Souny, "Reduction of the sensor number in distributed vector-antennas for 3d direction finding," in *15th International Symposium on Antenna Technology and Applied Electromagnetics*, IEEE, 2012.

[11] J. Duplouy and et al., "3d direction-of-arrival estimation using a wideband vector antenna," in *2018 IEEE International Symposium on Antennas and Propagation & USNC/URSI National Radio Science Meeting*, pp. 291–292, 2018.

[12] J. Duplouy, C. Morlaas, H. Aubert, P. Potier, and P. Pouliguen, "Wideband vector antenna for dual-polarized and three-dimensional direction-finding applications," *IEEE Antennas and Wireless Propagation Letters*, vol. 18, pp. 1572–1575, 2019.

[13] A. Musicant, B. Almog, N. Oxenfeld, and R. Shavit, "Vector sensor antenna design for vhf band," *IEEE Antennas and Wireless Propagation Letters*, vol. 14, 2015.

[14] A. Lemma, E. Deprettere, and A.-J. van der Veen, "Experimental analysis of antenna coupling for high-resolution doa estimation algorithms," in *2nd IEEE Workshop on Signal Processing Advances in Wireless Communications*, pp. 362–365, 1999.

[15] S. Chandran, *Advances in Direction-of-Arrival Estimation*. Artech, 2005.

[16] J. Lominé, C. Morlaas, C. Imbert, and H. Aubert, "Dual-band vector sensor for direction of arrival estimation of incoming electromagnetic waves," *IEEE Transactions on Antennas and Propagation*, vol. 63, no. 8, pp. 3662–3671, 2015.